

## Supplementary Information

# Highly Efficient UV-to-Red Light-Conversion LuNbO<sub>4</sub>:Eu<sup>3+</sup> Phosphors Through Exciton-Assisted Host-Activator Energy Transfer

*Fei Xiong<sup>a, b ‡</sup>, Wen Liu<sup>a ‡</sup>, Zuimin Jiang<sup>b</sup>, Zhu Zhu<sup>a</sup>, and Wanbiao Hu<sup>a \*</sup>*

<sup>a</sup> Yunnan Key Laboratory of Electromagnetic Materials and Devices, School of Materials and Energy, Yunnan University, Kunming 650091, PR China

<sup>b</sup> State Key Laboratory of Surface Physics and Department of Physics, Fudan University, Shanghai 200433, P. R. China

\*Email for Wanbiao Hu: huwanbiao@ynu.edu.cn

‡These authors contributed equally.

**Table S1** Refined Structure parameters of LNO:  $x\text{Eu}^{3+}$ 

Doping level	0.00	0.01	0.05	0.09	0.13	0.17	0.20	
$a$ (Å)	Values	5.226	5.229	5.236	5.241	5.246	5.253	5.257
	SD	0.001	0.001	0.002	0.001	0.002	0.001	0.001
$b$ (Å)	Values	10.820	10.825	10.835	10.849	10.859	10.872	10.881
	SD	0.002	0.002	0.003	0.003	0.001	0.001	0.001
$c$ (Å)	Values	5.039	5.041	5.043	5.047	5.049	5.053	5.055
	SD	0.001	0.001	0.001	0.001	0.001	0.001	0.001
$\alpha$ (°)	90	90	90	90	90	90	90	
$\beta$ (°)	94.412	94.405	94.399	94.418	94.424	94.424	94.427	
$\gamma$ (°)	90	90	90	90	90	90	90	
$R_p$ (%)	6.928	5.519	5.113	6.214	4.889	5.213	4.863	
$R_{wp}$ (%)	8.819	8.017	7.546	8.746	7.010	7.319	6.860	
$\chi^2$	4.809	7.781	6.344	3.443	4.531	4.155	3.626	

Here, SD refers to the standard deviation. The SD values of the calculated parameters  $\alpha$ ,  $\beta$ ,  $\gamma$  are less than 0.005 °. The refined parameters i.e.,  $R_p$  and  $R_{wp}$  finally converge to less than 10% as well as  $\chi^2$  is less than 10, indicating the refined results are reliable. The lattice constants  $a$ ,  $b$ ,  $c$  increase with the increasing of  $\text{Eu}^{3+}$  doping levels, indicating the host lattice expansion with the incorporation of  $\text{Eu}^{3+}$  ions.

**Table S2** Bond length and bond angle of LNO:  $x\text{Eu}^{3+}$ 

Doping level ( $x$ )	Bond angle Lu-O <sub>1</sub> -Lu (°)	Bond length (Å)						
		Lu-	Lu-	Lu-	Lu-	Nb-	Nb-	Lu-
0.00	106.951	2.371	2.289	2.344	2.279	1.924	1.844	3.716
0.01	106.972	2.372	2.290	2.345	2.280	1.926	1.845	3.718
0.05	106.994	2.374	2.291	2.346	2.281	1.928	1.846	3.720
0.09	107.026	2.376	2.293	2.349	2.283	1.931	1.847	3.725
0.13	107.051	2.378	2.295	2.351	2.285	1.933	1.849	3.728
0.17	107.078	2.381	2.298	2.354	2.288	1.935	1.851	3.733
0.20	107.096	2.383	2.299	2.355	2.289	1.936	1.852	3.736

The standard deviation (SD) values of the calculated bond length are less than 0.002 Å, and the SD values of the calculated bond angle are less than 0.007 °. The Lu-O<sub>1</sub>-Lu bond angle increases from 106.951° to 107.096 ° with increasing the Eu<sup>3+</sup> doping levels, as well, the In-O and La-O bond lengths and the Lu-Lu distance are also enlarged. However, different types of O atoms coordinating with Lu/Eu ions produce Lu/Eu-O bonds with different bond length, which results in the contorted LuO<sub>8</sub> dodecahedrons and an asymmetrical crystal field, and the expansion of LuO<sub>8</sub> dodecahedron is much larger than that of NbO<sub>4</sub> tetrahedrons. As a results of the structural change, the NbO<sub>4</sub> ditetrahedrons should become more isolated as the distance among them is lengthen.

**Table S3** Photoluminescence quantum yield (PLQY) of the previously-reported red phosphors which are doped optimally and excited by the light with the wavelength  $\lambda_{\text{ex}}$

Phosphor	$\lambda_{\text{ex}}$	PLQY	Reference
$\text{Na}_3\text{Sc}_2\text{Mg}(\text{PO}_4)_3: 0.30\text{Eu}^{3+}$	350 nm	88.3%	[1]
$\text{La}_7\text{Ta}_3\text{W}_4\text{O}_{30}: 0.20\text{Eu}^{3+}$	397 nm	85.85%	[2]
$\text{Gd}_{3.67}\text{EuSi}_3\text{O}_{13}$	394 nm	82.1%	[3]
$\text{LuNbO}_4: 0.09\text{Eu}^{3+}$	248 nm	76.3%	This work
$\text{Ca-}\alpha\text{-SiAlON}: 0.03\text{Eu}^{2+}$	455 nm	70.5%	[4]
$\text{BaMgAl}_{11}\text{O}_{19}: 0.02\text{Eu}^{2+}$	450 nm	60%	[5]
$\text{YPO}_4: 0.10\text{Eu}^{3+}$	395 nm	60%	[6]
$\text{GdNbO}_4: 0.001\text{Eu}^{3+}$	260 nm	59.7%	[7]
$\text{Ca}_2\text{YNbO}_6: 0.20\text{Eu}^{3+}$	396 nm	56.23%	[8]
$\text{CaAlSiN}_3: 0.01\text{Ce}^{3+}$	460 nm	56%	[9]
$\text{SrAl}_2\text{O}_4: 0.20\text{Eu}^{2+}$	420 nm	55%	[10]
$\text{LaNbO}_4: 0.005\text{Eu}^{3+}$	261 nm	41.9%	[11]
$\text{CaNb}_2\text{O}_6: 0.03\text{Eu}^{3+}$	265 nm	35.6%	[12]

The PLQY of 76.3%, exceeding most of previously reported values in other materials, is obtained when  $\text{LNO}: 0.09\text{Eu}^{3+}$  phosphors are excited with 248nm light. Some previous reports have presented some other excitation methods for generating red photoluminescence, by which the measured PLQY can also be quite large, but the luminescence external quantum efficiency (EQE) is rather small. The disappointing values of EQE should come from the poor absorptivity to the excitation source. In current  $\text{LNO}: x\text{Eu}^{3+}$  phosphors,  $\text{Eu}^{3+}$  ions obtain the excitation energy by the host absorptance to the pumping photons and energy transfer. The absorptivity to

248 nm light is up to 87.5 %, and the efficiency of energy transfer also reaches 92.8 %, which result in an extremely large EQE of 66.8 % in LNO: 0.09Eu<sup>3+</sup> phosphors.

**Table S4** Luminescence colorimetric properties including CIE, CCT and CP for LNO:  $x\text{Eu}^{3+}$  phosphors under 248 nm excitation at room temperature

Doping level ( $x$ )	CIE coordinate ( $x, y$ )	CCT (K)	CP (%)
0.01	(0.4413, 0.2318)	3680.20	42.17
0.03	(0.5718, 0.3041)	2763.09	70.82
0.05	(0.6042, 0.3204)	2752.06	79.51
0.07	(0.6264, 0.3302)	2790.96	85.59
0.09	(0.6369, 0.3320)	2903.76	88.45
0.11	(0.6433, 0.3341)	2937.39	90.20
0.13	(0.6434, 0.3359)	2877.12	90.26
0.15	(0.6505, 0.3363)	2958.47	92.18
0.17	(0.6533, 0.3376)	2980.99	92.96
0.20	(0.6550, 0.3376)	3009.20	93.42

The emission color of LNO:  $x\text{Eu}^{3+}$  is tuned by the  $\text{Eu}^{3+}$ -doping-related energy transfer. For the undoped LNO, only the STE blue emission was observed. The  $\text{Eu}^{3+}$  incorporation results in the exciting energy transferred from host to  $\text{Eu}^{3+}$  ions, which reduces the blue emission intensity of STE while the red luminescence of  $\text{Eu}^{3+}$  ions is enhanced. As a result, the CP for red emission increases gradually as increasing the doping level  $x$ , and the luminescence CCT decreases to the values below 3000 K. For LNO:  $0.09\text{Eu}^{3+}$  that exhibits the highest luminescence external quantum efficiency among these doped phosphors, the red emission CP can reach a large value of 88.45%.

**Table S5** CIE chromaticity coordinates (x, y) and color correlated temperature (CCT) of the luminescence from LNO: 0.09Eu<sup>3+</sup> under 248 nm excitation at different temperature

Temperature (K)	CIE coordinate (x, y)	CCT (K)	CP (%)
298	(0.6397, 0.3320)	2093.76	88.45
328	(0.6401, 0.3325)	2897.56	89.56
358	(0.6405, 0.3335)	2877.14	89.70
388	(0.6414, 0.3352)	2854.87	89.92
418	(0.6436, 0.3358)	2833.36	90.51
448	(0.6454, 0.3360)	2801.58	91.03.
478	(0.6419, 0.3371)	2820.65	90.08

The luminescence colorimetric characteristics have changed little as temperature increases from 298 K to 478 K. Especially, the CIE chromaticity coordinates for LNO: 0.09Eu<sup>3+</sup> calculated from the emission spectra measured at 298-478 K are almost overlapped with each other, revealing that the emission colors are almost not changed with the temperatures.

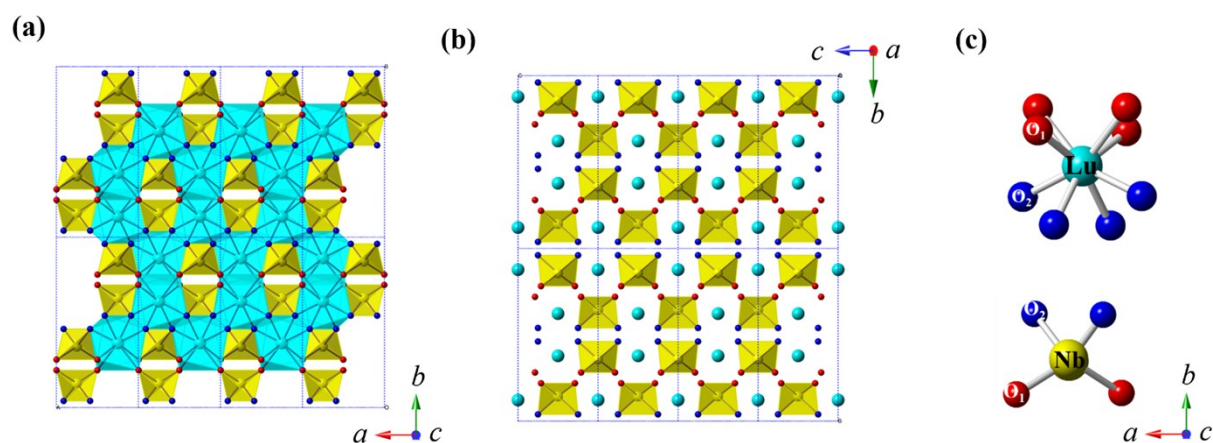


**Figure S1** Schematic Diagram of the LNO crystal structure (a) along the  $c$ -axis, (b) along the  $a$ -axis; (c) Schematic diagrams of LuO<sub>8</sub> and NbO<sub>6</sub> polyhedrons.

The crystal consists of the distorted NbO<sub>4</sub> tetrahedrons and the contorted LuO<sub>8</sub> dodecahedrons. Two adjacent LuO<sub>8</sub> dodecahedrons are connected in a side-sharing type, and then these connected dodecahedrons formed a network. Two adjacent NbO<sub>4</sub> tetrahedrons which connect through Nb-O1-O1-Nb bond, form a ditetrahedron. All the ditetrahedrons are separated by the LuO<sub>8</sub> net, and exhibit the zero-dimensional features. The substructure along the direction of  $c$  axe is mainly composed of a NbO<sub>4</sub> chain, while the LuO<sub>8</sub> units dominate the  $ab$  plane, thus the expansion of LuO<sub>8</sub> dodecahedron caused by the substitution for Lu<sup>3+</sup> with larger Eu<sup>3+</sup>, causes the anisotropic structure change. As a results, the NbO<sub>4</sub> ditetrahedrons become more isolated as the distance among them is lengthen.

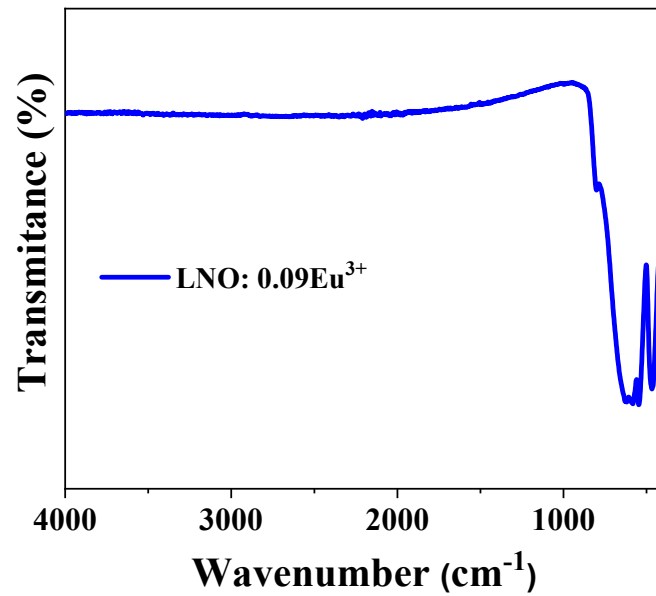


**Figure S2** FTIR absorption spectrum of LNO: 0.09Eu<sup>3+</sup> in the range of 400-4000 cm<sup>-1</sup>. No peaks related with C-H, O-H and H<sub>2</sub>O are detected. These C/O/H species are easily molecularly absorbed at the subsurface region of oxygen deficiency. The FTIR absorption spectrum implies less oxygen defect on the sample surface.

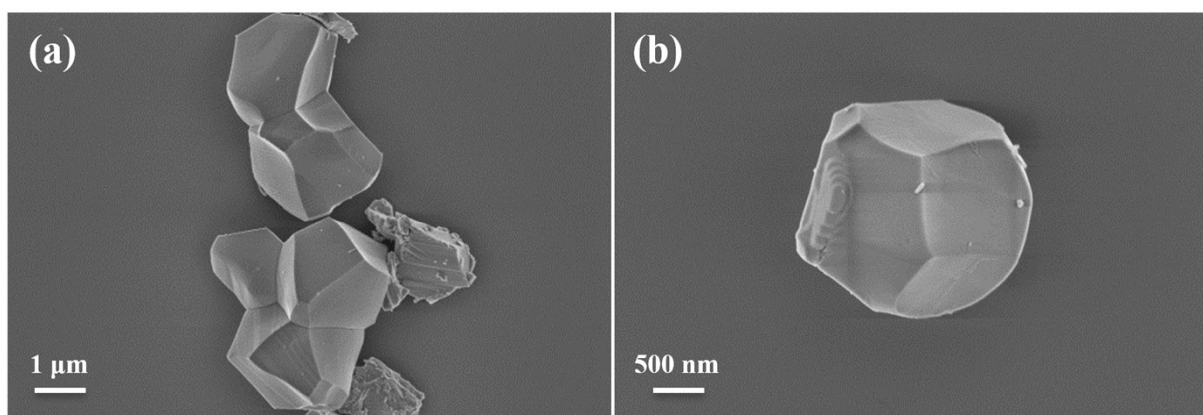


**Figure S3** FE-SEM images of LNO: 0.09Eu<sup>3+</sup>. (a) the aggregated polycrystals, and (b) a single crystallized particle. The crystal grains with the uniform size in the range of 1-2 μm exhibit the smooth surface and the sharp edges, demonstrating the perfect crystallization of the phosphors.

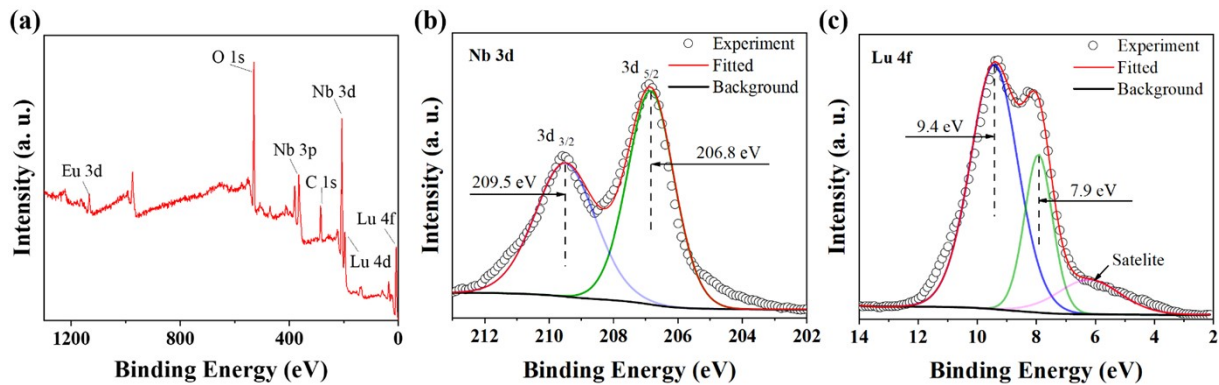


**Figure S4** XPS spectra of (a) survey of scan, (b) Nb 3d core level, (c) Lu 4f core level of the LNO: 0.09Eu<sup>3+</sup> phosphor.

XPS spectrum in Figure S4a confirms that the as-prepared phosphors are only composed of Lu, Nb, Eu and O elements. The core level spectra of Lu and Nb indicate that they exist in the oxidation state with chemical valence of +3, +5, respectively.

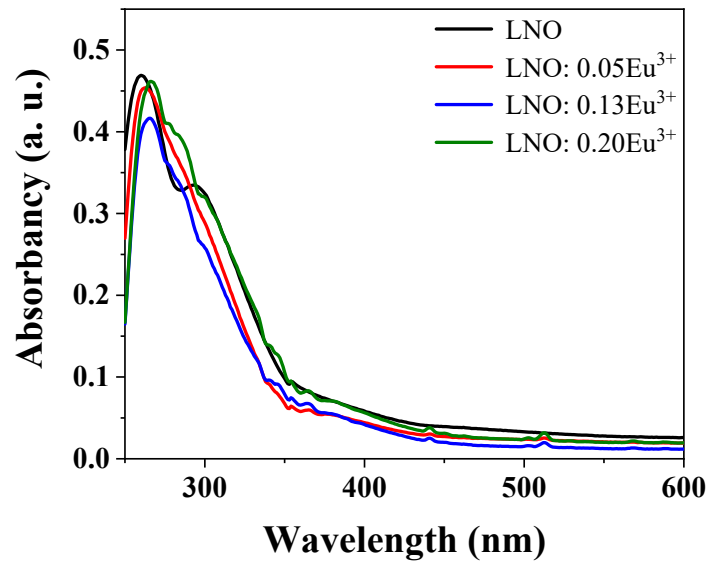


**Figure S5** UV-Vis absorption spectra of LNO:  $x\text{Eu}^{3+}$  ( $x = 0, 0.05, 0.13, 0.20$ ) samples in the range of 250-600 nm.

The UV-Vis absorption spectra of LNO:  $x\text{Eu}^{3+}$  phosphors, similar to that of the undoped host, also present two distinct absorption bands in the wavelength range of the 250-300 nm and 300-350 nm respectively, indicating the two types of electronic transitions from ground state to excited state. According to the UV-Vis absorption spectra of LNO:  $x\text{Eu}^{3+}$  phosphors, the electronic band structure of LNO host seems no significant change after incorporation of the  $\text{Eu}^{3+}$  ions

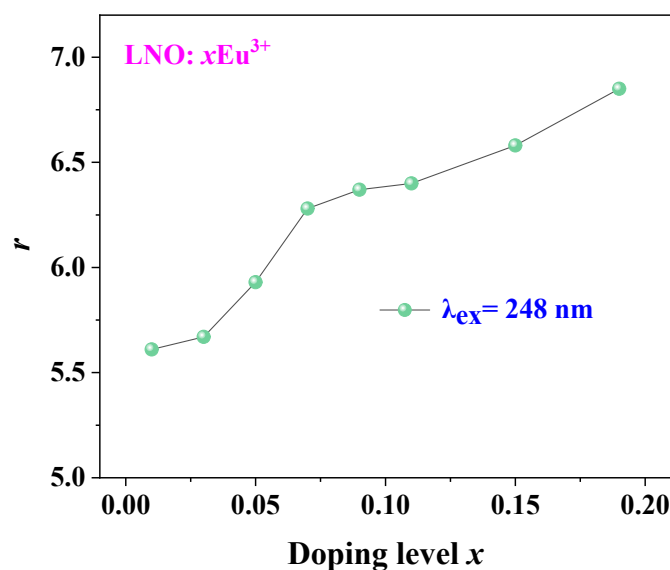


**Figure S6** Doping dependence of the integrated-intensity ratio  $r$  between the emission caused by the electric dipole transition  ${}^5D_0 \rightarrow {}^7F_2$  and the emission due to the magnetic dipole transition  ${}^5D_0 \rightarrow {}^7F_1$ .

When  $\text{Eu}^{3+}$  ions are located at a non-centrosymmetric lattice site, the emission at 613 nm which comes from the electric dipole transition  ${}^5D_0 \rightarrow {}^7F_2$  will dominate the  $\text{Eu}^{3+}$  luminescence. However, when  $\text{Eu}^{3+}$  ions are located at a centrosymmetric lattice site, the emission at 595 nm which comes from the magnetic dipole transition  ${}^5D_0 \rightarrow {}^7F_1$  will become much stronger. Therefore, the integrated intensity ratio ( $r$ ) between the  ${}^5D_0 \rightarrow {}^7F_2$  luminescence and  ${}^5D_0 \rightarrow {}^7F_1$  emission should reflect the asymmetry degree of the crystal field surrounding the  $\text{Eu}^{3+}$  ions. The ratio exhibits the larger values in the higher doped phosphors when  $\text{LuNbO}_4: x\text{Eu}^{3+}$  is excited with the 248 nm light, indicating that the symmetry degree of the crystal field surrounding the  $\text{Eu}^{3+}$  ions is reduced with the  $\text{Eu}^{3+}$  concentration increasing.

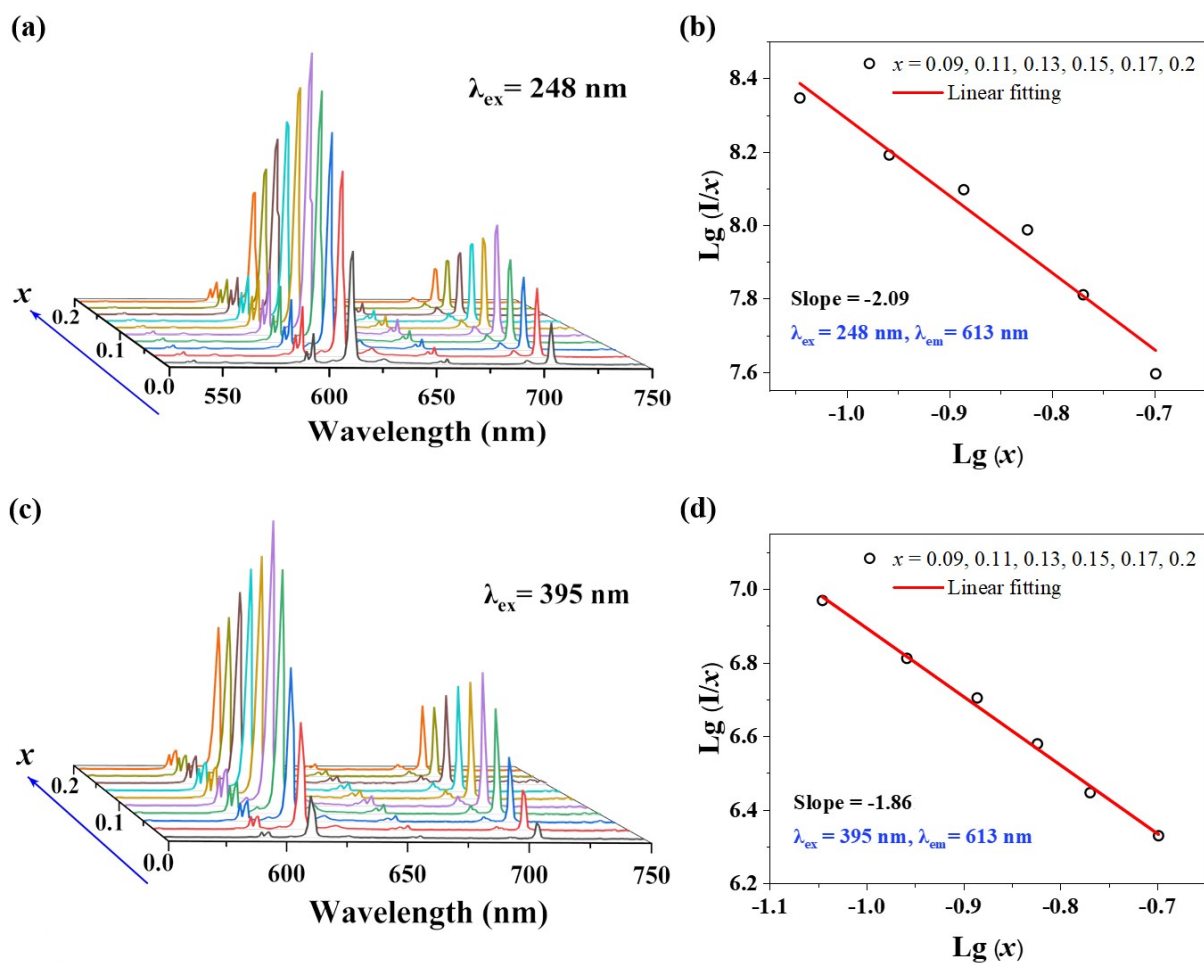


**Figure S7** Performance of  $\text{Eu}^{3+}$  luminescence in  $\text{LNO}: x\text{Eu}^{3+}$  phosphors. (a)  $\text{Eu}^{3+}$  luminescence spectra of  $\text{LNO}: x\text{Eu}^{3+}$  on 248 nm excitation. (b) Variation of  $\log(I/x)$  vs.  $\log x$  for the luminescence excited by 248 nm light. Here,  $I$  refers to the luminescence intensity. (c)  $\text{Eu}^{3+}$  luminescence spectra of  $\text{LNO}: x\text{Eu}^{3+}$  on direct excitation of 395 nm light. (d) Linear relationship of  $\log(I/x)$  vs.  $\log x$  for the luminescence excited by 395 nm light.

The  $\text{Eu}^{3+}$  luminescence exhibits similar doping dependence in spite of the different excitation ways. With increasing the  $\text{Eu}^{3+}$  doping level  $x$ , the luminescence intensity firstly increases and reaches the maximum at  $x = 0.09$ , and then decreases with a further increasing  $x$  (Figure S7a and Figure S7c). Since the increase of doping levels reduces the distance between  $\text{Eu}^{3+}$  ions, the interaction between the  $\text{Eu}^{3+}$  ions will be enhanced. When the distance is getting

close enough, the excited 4f electrons will be relaxed through the exchange interaction among the neighboring  $\text{Eu}^{3+}$  ions, and the concentration quenching (CQ) effect will occur. According to the Blasse theory, the critical distance  $R_c$  for CQ effect can be calculated: <sup>[13]</sup>

$$R_c = 2 \left( \frac{3V}{4\pi Z x_c} \right)^{\frac{1}{3}} \quad (S1)$$

where  $V$  is the volume of the unit cell,  $x_c$  is the critical doping level, and  $Z$  represents the cation number in the host unit cell. For LNO:  $x\text{Eu}^{3+}$  phosphors,  $x_c=0.09$ ,  $Z=4$ , therefore, the critical distance  $R_c$  is calculated to be about 11.47 Å.

The way of multilevel energy transfer among  $\text{Eu}^{3+}$  ions, can be further explored by the Reisfeld's approximation and Dexter's energy transfer theory following: <sup>[14, 15]</sup>

$$\frac{I}{x} = k \left[ 1 + \beta(x)^{\frac{\theta}{3}} \right]^{-1} \quad ( S 2 )$$

Where  $x$  and  $I$  are the doping level and the luminescence intensity of  $\text{Eu}^{3+}$  ions,  $k$  and  $\beta$  are constant. The  $\theta$  is dependent on the way of electric interaction between the neighboring  $\text{Eu}^{3+}$  ions such as dipole-dipole, dipole-quadrupole, and quadrupole-quadrupole interactions. The variation of  $\log(I/x)$  vs.  $\log(x)$  plot can be fitted linearly with giving the slope equal to  $\theta/3$ . As demonstrated in Figure S7b and Figure S7d, the  $\theta$  is estimate to be 6.29 when the phosphors are excited by 248 nm light, and 5.58 when the phosphors are under direct excitation of 395 nm light. Both of them approach 6. Therefore, the CQ effect is caused by the electric dipole-dipole interaction when the  $\text{Eu}^{3+}$  doping level  $x \geq 0.09$ .

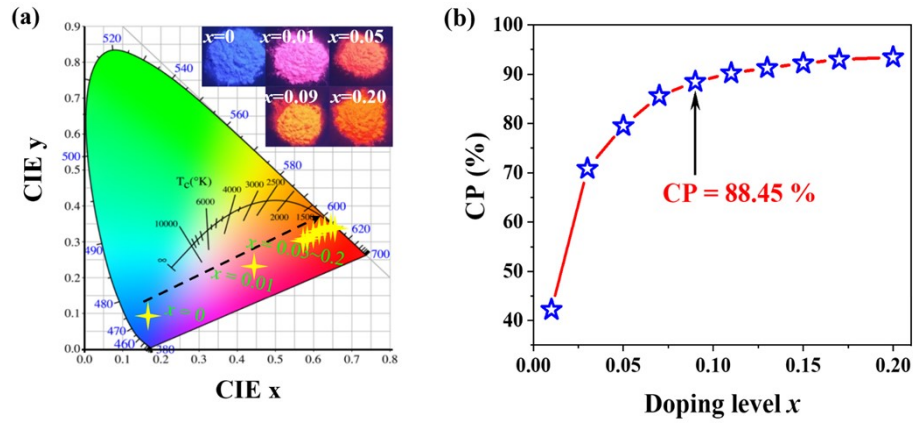


**Figure S8** (a) CIE chromaticity coordinates of LNO:  $x\text{Eu}^{3+}$  emission under 248 nm excitation. The inset displays the luminescence photograph of LNO:  $x\text{Eu}^{3+}$  on 255 nm excitation. (b) Doping dependent CP values for luminescence of the LNO:  $x\text{Eu}^{3+}$  phosphors.

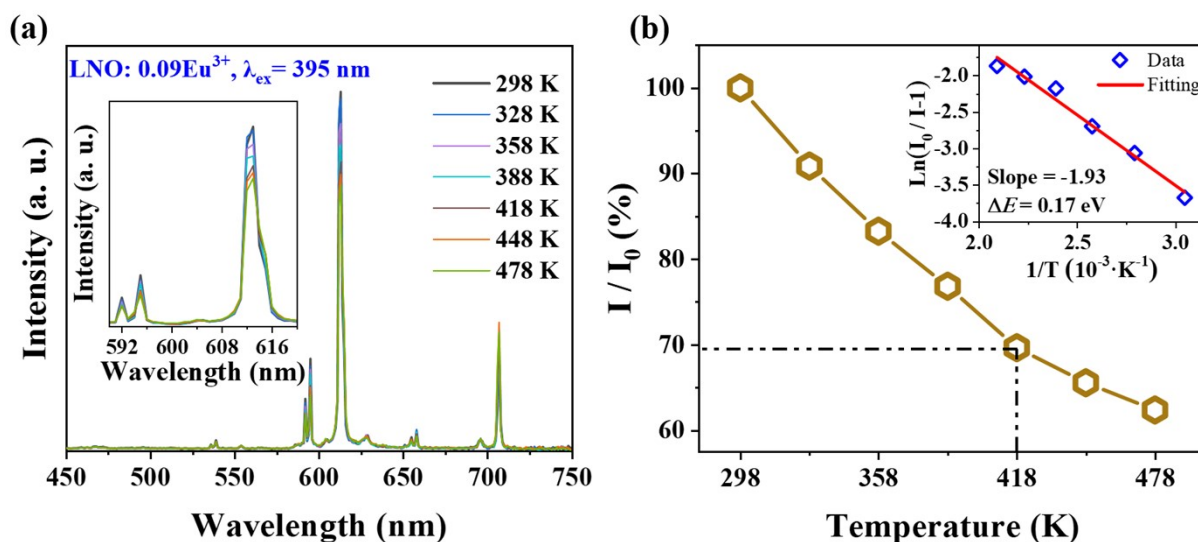


**Figure S9** PL thermal stability of LNO: 0.09Eu<sup>3+</sup> phosphor on excitation of 395 nm. (a) PL spectra at different temperature. The enlarged spectra in the range from 590 nm to 620 nm are also shown in the inset. (b) Temperature dependence of the normalized PL intensity. The inset presents the  $\ln[(I_0/I)-1]$  vs.  $1/T$  plot for the determination of the activation energy  $\Delta E$  of thermal quenching.

A remarkably thermal quenching effect of Eu<sup>3+</sup> luminescence is observed in LNO: 0.09Eu<sup>3+</sup> phosphor under the direct excitation of 395 nm light. The lighting process does not involve the energy transfer. As the temperature increases from 298 K to 478 K, the luminescence intensity decreases gradually. The calculated  $\Delta E$  is about 0.17 eV.

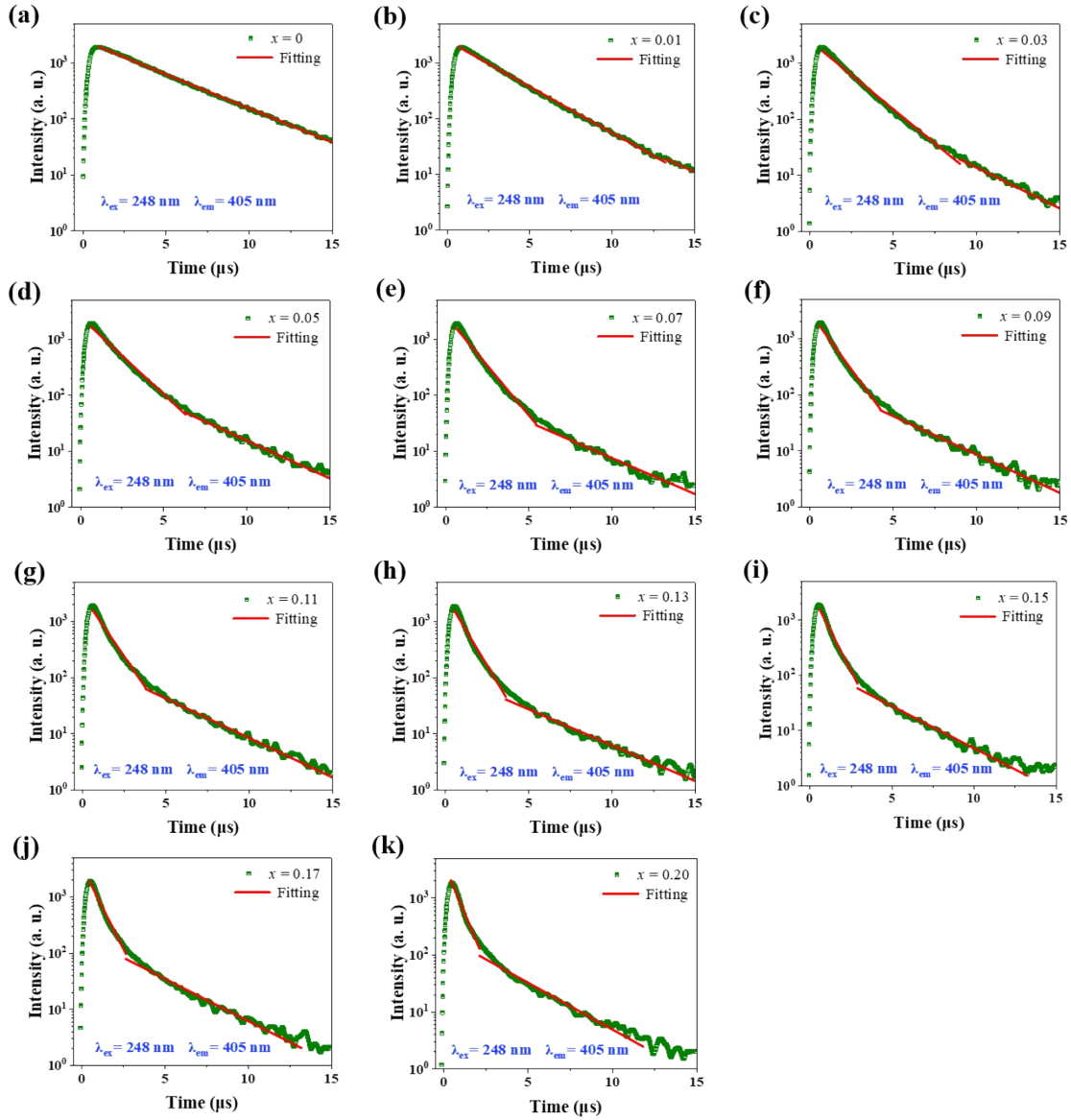


**Figure S10** Fluorescence decay curves of LNO:  $x\text{Eu}^{3+}$  phosphors monitored at 405 nm under 248 nm excitation. (a)  $x = 0$ , (b)  $x = 0.01$ , (c)  $x = 0.03$ , (d)  $x = 0.05$ , (e)  $x = 0.07$ , (f)  $x = 0.09$ , (g)  $x = 0.11$ , (h)  $x = 0.13$ , (i)  $x = 0.15$ , (j)  $x = 0.17$ , (k)  $x = 0.20$ .

Although the decay performance of exciton emission is consistent with the single exponential equation in the undoped LNO, the PL decay behaviors for the  $\text{Eu}^{3+}$  doped phosphors have to be depicted with a double exponential function, i.e.,  $I = A_1 \cdot \exp(-t/\tau_1) + A_2 \cdot \exp(-t/\tau_2)$ . Here,  $\tau_1$  and  $\tau_2$ , representing the luminescence life time, decrease with the  $\text{Eu}^{3+}$  doping level  $x$ .

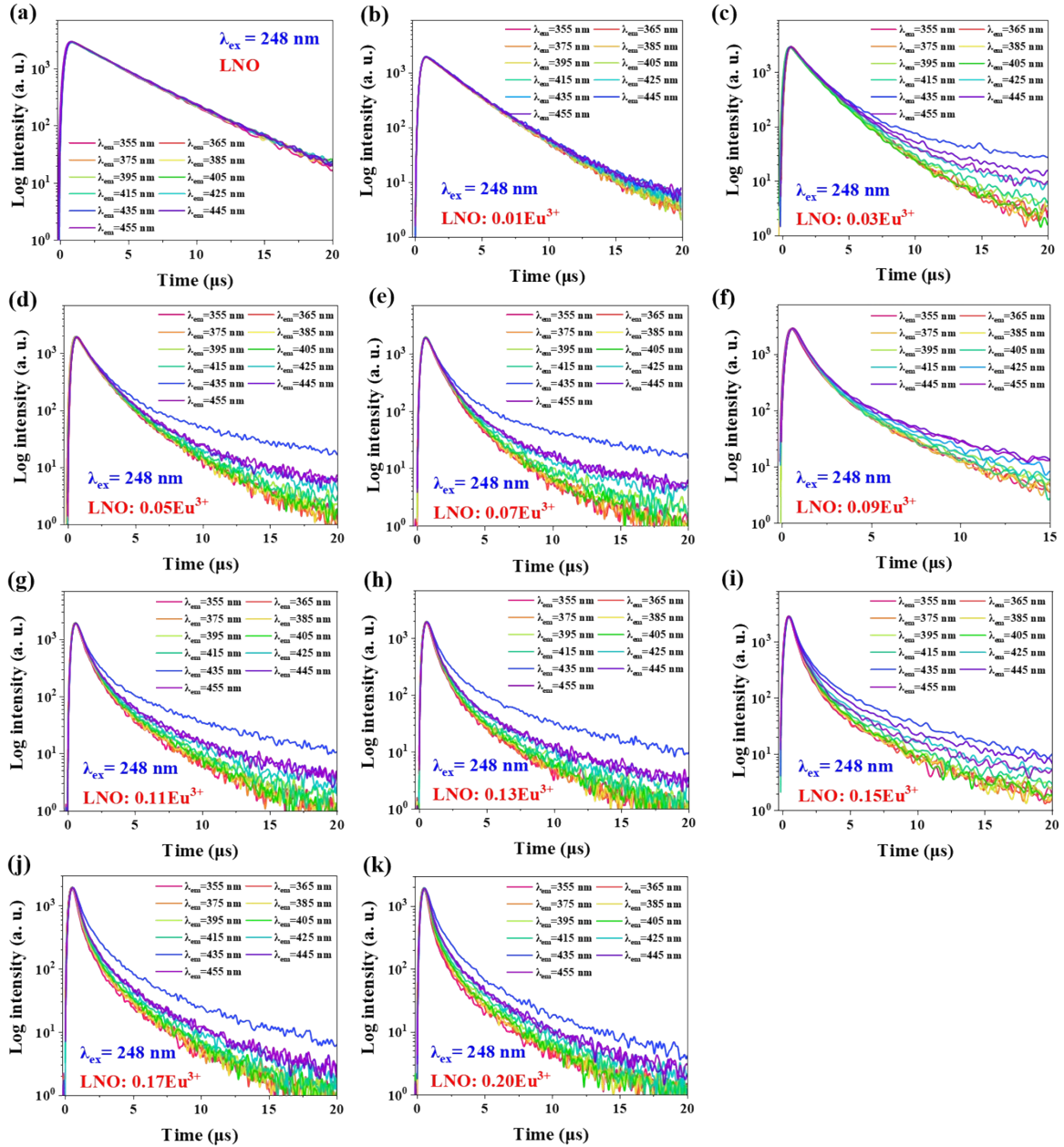


**Figure S11** Time-resolved exciton emission spectra monitored at the wavelengths in the region from 350-455 nm when LNO:  $x\text{Eu}^{3+}$  are excited by the 248 nm light. (a)  $x = 0$ , (b)  $x = 0.01$ , (c)  $x = 0.03$ , (d)  $x = 0.05$ , (e)  $x = 0.07$ , (f)  $x = 0.09$ , (g)  $x = 0.11$ , (h)  $x = 0.13$ , (i)  $x = 0.15$ , (j)  $x = 0.17$ , (k)  $x = 0.20$ .

When the phosphors are excited by the 248 nm light, the decay curves monitored at any wavelengths in the emission band of 350-455 nm can be fitted with the almost same  $\tau_1$  and  $\tau_2$ .

## REFERENCES

- (1) H. Zhang, Y. Su, Z. Luo, J. Zhang, J. Yang, *ACS Sustain. Chem. Eng.*, 2021, **9**, 785.
- (2) Y. Ren, B. Deng, T. Liang, S. Shu, J. Guo, S. Zhao, R. Yu, *J. Rare Earths*, 2021, **39**, 905.
- (3) W. Ye, C. Zhao, X. Shen, C. Ma, Z. Deng, Y. Li, Y. Wang, C. Zuo, Z. Wen, Y. Li, X. Yuan, C. Wang, Y. Cao, *ACS Appl. Electron. Mater.*, 2021, **3**, 1403.
- (4) S. Yamada, H. Emoto, M. Ibukiyama, N. Hirosaki, *J. Eur. Ceram. Soc.*, 2012, **32**, 1355.
- (5) A. STEVELS, A. SCHRAMADEPAUW, *J. Electrochem. Soc.*, 2021, **123**, 691.
- (6) S. Rodrigue, F. J. Aparicio, T. C. Rojas, A. B. Hungria, L. E. Chinchilla, M. Ocana, *Cryst. Growth Des.*, 2011, **12**, 635.
- (7) X. Liu, C. Chen, S. Li, Y. Dai, H. Guo, X. Tang, Y. Xie, L. Yan, *Inorg. Chem.*, 2016, **55**, 10383.
- (8) Y. Hua, W. Ran, J. S. Yu, *ACS Sustain. Chem. Eng.*, 2021, **9**, 7960.
- (9) Y. Li, N. Hirosaki, R. Xie, *Chem. Mater.*, 2008, **20**, 6704.
- (10) F. Meister, M. Batentschuk, S. Dröscher, A. Osvet, A. Stiegelschmitt, M. Weidner, A. Winnacker, *Radiat. Meas.*, 2007, **42**, 771.
- (11) K. Li, Y. Zhang, X. Li, M. Shang, H. Lian, J. Lin, *Phys. Chem. Chem. Phys.*, 2015, **17**, 4283.
- (12) K. Li, X. Liu, Y. Zhang, X. Li, H. Lian, J. Lin, *Inorg. Chem.*, 2015, **54**, 323.
- (13) G. Blasse, *Phys. Lett. A*, 1968, **28A**, 444.
- (14) D. L. Dexter, J. H. Schulman, *J. Chem. Phys.*, 1954, **22**, 1063.
- (15) J. Zhu, J. Xiang, D. Yang, Z. Fang, Y. Zheng, Y. Mao H. Zhao, *Ceram. Int.*, 2020, **46**, 844.